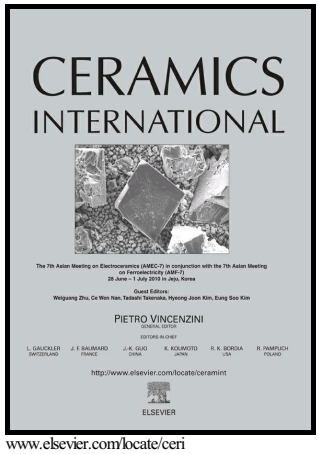

www.elsevier.com/locate/ceri

Surface structural and solar absorptance features of nitrate-based copper-cobalt oxides composite coatings: Experimental studies and molecular dynamic simulation

Amun Amri, Ahmad Fadli, Zhong-Tao Jiang, Chun-Yang Yin, M. Mahbubur Rahman, Hantarto Widjaja, Syamsu Herman, Silvia Reni Yenti, M. Miftahul Munir, Gadang Priyotomo, M. Iqbal, Neni Frimayanti

PII: S0272-8842(18)31317-8
DOI: https://doi.org/10.1016/j.ceramint.2018.05.171
Reference: CERI18346

To appear in: *Ceramics International*

Received date: 18 April 2018
Accepted date: 19 May 2018

Cite this article as: Amun Amri, Ahmad Fadli, Zhong-Tao Jiang, Chun-Yang Yin, M. Mahbubur Rahman, Hantarto Widjaja, Syamsu Herman, Silvia Reni Yenti, M. Miftahul Munir, Gadang Priyotomo, M. Iqbal and Neni Frimayanti, Surface structural and solar absorptance features of nitrate-based copper-cobalt oxides composite coatings: Experimental studies and molecular dynamic simulation, *Ceramics International,* https://doi.org/10.1016/j.ceramint.2018.05.171

Surface structural and solar absorptance features of nitrate-based copper-cobalt oxides composite coatings: Experimental studies and molecular dynamic simulation

Amun Amri[a*], Ahmad Fadli[a], Zhong-Tao Jiang[b*], Chun-Yang Yin[c*], M. Mahbubur Rahman[b,d], Hantarto Widjaja[b], Syamsu Herman[a] , Silvia Reni Yenti[a], M. Miftahul Munir[e] , Gadang Priyotomo[f], M. Iqbal[a], Neni Frimayanti[g]

[a]Department of Chemical Engineering, Universitas Riau, Pekanbaru, Indonesia
[b]Surface Analysis and Materials Engineering Research Group, School of Engineering & Information Technology, Murdoch University, Murdoch, WA 6150, Australia
[c]Newcastle University in Singapore, 537 Clementi Road #06-01, SIT Building @ Ngee Ann Polytechnic, Singapore 599493
[d]Department of Physics, Jahangirnagar University, Savar, Dhaka 1342, Bangladesh
[e]Department of Physics, Institut Teknologi Bandung (ITB), Jl. Ganesha Bandung, Indonesia
[f]Indonesian Institute of Sciences (LIPI), Serpong, Tangerang, Indonesia
[g]College of Pharmaceutical Sciences Riau (STIFAR), Pekanbaru, Indonesia
amun.amri@eng.unri.ac.id
M.Rahman@Juniv.edu
M.Rahman@Murdoch.edu.au
[*]Corresponding authors. Tel./fax.: +62 761 566 937.

Abstract

The copper and cobalt oxides composites coatings on aluminum substrates have been successfully synthesized *via* sol-gel method using nitrate-based sol precursors. The composites were characterized by X-ray Diffraction (XRD), X-ray photoelectron spectroscopy (XPS), Field Emission Scanning Electron Microscopy (FESEM), Atomic Force Microscopy (AFM), and UV-Vis-NIR spectrophotometry. The sol-gel reactions were discussed and Molecular Dynamics (MD) simulation was integrated into the study to predict molecules assembly properties. The XRD analyses revealed that the CuO and the Co_3O_4 composites were formed after the annealing process with the average difference of the calculated lattice parameters compared to ICDDs was 1.17%. The surface electronic structure was mainly consisted of tetrahedral Cu(I), octahedral Cu(II), tetrahedral Co(II), octahedral Co(III) as well as surface, sub-surface and lattice oxygen O^-. The XRD, XPS and MD simulation results showed that there was minimal (or possibly non-existing) indication of copper-cobalt mixed phase oxides formations. FESEM and AFM surveys revealed that the coating had a porous surface composed of interlinked nanoparticles in the range of ~10 to ~40 nm. UV-Vis-NIR reflectance spectra showed that the sol precursors concentration and the dip-drying cycle significantly influenced the absorptance value with optimum absorptance (α) of 88.7% exhibited by coating synthesized using sol concentration of 0.1 M and 10 dip-drying cycles. High absorptance value and simplicity in the synthesis process render the coatings to be very promising candidates for solar selective absorber (SSA) applications.

Keywords

Copper cobalt oxides, nitrate, sol-gel, structural, absorptance, coatings

1. Introduction

Copper oxide, cobalt oxide and their composite/mixture oxides have been known to exhibited a wide range applications such as catalysts, semiconductor, battery, capacitor, and sensor *etc* [1-4]. Highly tunable properties of these oxides are due to their unique crystallite structures and special band gap energy as well as superior ion transport. They can accommodate and distribute the cations from various oxidation states within the available octahedral and tetrahedral sites of the close-packed planes [2, 5]. CuO (tenorite) is one of the most important catalysts and is known as the most stable in copper oxides family compared to the Cu_2O and Cu_3O_4 [2, 6]. In the nanoscale, the reduction and reactivity of the CuO depend on the shape and the exposed crystal planes. In this case, the surface lattice oxygen plays an important role [6]. Co_3O_4 has been widely applied in the field of capacitance due to its high reversible capacity and simple preparation compared to other types of cobalt oxides (CoO, Co_2O_3) [5].

The diffussion of copper ions into Co_3O_4 structure by partially replacement of the cobalt ions, results in a well-ordered mesoporous crystalline mixed $CuCo_2O_4$ spinel cobaltites compound. This has attracted much attention since it is capable of reversible reaction with lithium. It could involve an alloying-dealloying mechanism forming promising anode materials in lithium ion battery (LIB) applications [5, 7]. Moreover, in terms of catalytic properties, the copper cobaltites compounds ($Cu_xCo_{3-x}O_4$) also possess superior performance in catalytic applications even in a low temperature process, exceeding the Co_3O_4 and CuO as well as stable in oxidation states [1]. This could be related to the high density of cation vacancy in these cobaltites. The thermal durability and optical properties of CuCo-oxide thin film coatings fabricated together with a SiO_2 antireflection layer was reported in an earlier study [8].

Absorptance is a key parameter in solar selective absorber (SSA) applications in determining the amount of energy could be absorbed by surface when subjected to a light source. In this work, we have investigated the structural and absorptance properties of copper cobalt oxides composites on aluminum substrates synthesized via sol-gel method using nitrate-based precursors, which are rarely studied in relation to their absorptance properties. It is generally well-established that the sol precursors concentration and the dip-drying cycle significantly influenced the absorptance. The optimum absorptance value of α = 88.7% achieved in this

work exceeds that of the sol-gel SSA coating (before the addition of anti-reflection layer), namely α = 87% as reported by Bayon and co-researchers [9].

2. Experimental

2.1. Preparation of thin film coatings

Copper (II) nitrate trihydrate ($Cu(NO_3)_2.3.H_2O$ (Merck), cobalt (II) nitrate hexahidate ($Co(NO_3)_{2.}6H_2O$), propionic acid (C_2H_5COOH) and absolute ethanol (Merck) were used as received. The commercial aluminium plates (Anofol) sizes of 2×4 cm^2 were used as substrates. Copper nitrate and cobalt nitrate powder, catalyst/coplexing agent of propionic acid and absolute ethanol were mixed and stirred for 2 hours to form 0.1 M sol precursor with [Cu]/[Co] molar ratio of 1.0. The sol solutions were then used for thin film deposition on aluminum substrates via dip-coating at withdrawal rate of 750 mm/min and subsequently heated at 150 °C for 1 min. For absorptance analyses, the copper-cobalt thin films with various densities and thicknesses were prepared by varying of cobalt and copper sol precursor concentrations and the dip-heating cycles. To study the effect of porosity on the absorptance properties, the coatings were also deposited on substrate Al using Nachriebe 600 electrospinning machine. Polyvinyl alcohol (PVA) 10% was used as driver solution with 12 kV voltage, 18µL/min flowrate and plate to tip-needle distance of 10 cm. All coatings were finally annealed in oven furnace at temperature 550 ^oC for 1 hour. Annealing at other temperatures (750 ^oC and 950 ^oC) was also carried out to investigate the structure stability. For structural stability study, copper substrates were used.

2.2. Characterizations and simulation

Mineralogical characteristics of the thin films were analyzed by using X-ray Diffractometer (XRD) equipped with a Lynx-Eye detector and a Cu-tube. The lattice parameters of phases detected in XRD spectra were calculated using Dmol3 code[10], GGA-PBE functional[11], Grimme DFT-D correction [12], unrestricted spin, DFT semi-core pseudopotential, DND version 4.4 basis set, orbital cutoff of 4.0 Å, octupole multipolar expansion, energy tolerance of 2.69 meV, force tolerance of 0.54 eV/Å, and a smearing of 0.27 eV. The surface electronic structure of samples were probed using Kratos Axis Ultra XPS spectrometer (Manchester, UK) with Al-$K\alpha$ radiation (hv = 1486.6 eV). The samples were mounted horizontally onto sample holder and normal to the electrostatic entrance lens, using double-sided Cu sticky

tape. The CASA XPS (V.2.3.15) software was utilized for quantification analysis with Shirley background subtraction.

The surface morphology was explored using field emission scanning electron microscopy (FESEM) (Zeiss Neon 40EsB). The charging effects on the samples were minimized *via* Pt thin coatings. The high voltage field emission gun was settled at 5 kV. The surface topography of samples was investigated by Atomic Force Microscope (AFM) (Ntegra Prima, NT-MDT Co., Moscow, Russia) in semi-contact mode. A tetrahedral tip was used on a rectangular cantilever whereas the resonant frequency of 100–400 kHz and force constant of 3.0 – 40.0 N/m were applied. Solar absorptance was calculated based on the AM1.5 solar spectrum standard via reflectance spectrum recorded from 300 to 2650 nm using UV-Vis-NIR Jasco V-670 double beam spectrophotometer with 60 mm integrating sphere.

The Molecular Dynamic (MD) simulation was conducted to predict the stability of copper cobalt oxides coating through the ionization process of molecule bonds: Co-O-Co, Cu-O-Co and Cu-O-Cu. MD plays an important role in addresing a number of machining problems at atomic scale. In addition, the calculations may also shed a light on the "best" molecular force-field; thermo physical properties and vibration frequencies, which is invaluable in force-field development and refinement [13, 14]. In this work, preliminary study of molecular dynamic simulation was executed using NAMD (NAnoscale Molecular Dynamics program v 2.9). The selected force field of CHARMM19 (Chemistry at HARvard Macromolecular Mechanics) was used as the best force field, NPA (Nose-Poincare-Andersen) was then used as algorithm and NVT was used as ensemble parameter [14].

3. Results and discussion

3.1. Mineralogical analysis

Fig. 1 shows the mineralogical pattern of coatings on copper substrate synthesized at different annealing temperatures. Based on the intensities main peaks and the *d*-spacing analyses, the peaks at 2θ around of 35.49° (-111), 38.73° (111), and 48.73° (-202) are identified as CuO (Tenorite) (ICDD 00-045-0937), while the main peaks at 36.78° (311), 44.73° (400) and 59.25° (511) are due to the Co_3O_4 spinel structure (ICDD 01-080-1533). Generally, the highest peak intensities occur at annealing temperature of 750 °C, while it is conversely true for lower peak intensities at temperatures of 550 ^{o}C and 950 ^{o}C. The mean crystallite size of

the main peaks, calculated using Scherrer equation, increases with the increase of annealing temperature, namely 5.36, 6.18 and 13.43 nm at annealing temperatures of 550, 750 and 950 ^{o}C, respectively.

The lattice parameters of CuO and Co_3O_4 calculated using Dmol3 code are presented in Table 1, while the unit cells of CuO and Cu_3O_4 are depicted in Fig. 2. From Table 1, it can be seen that the average difference of the calculated lattice parameters compared to ICDDs is 1.17%. From Fig. 2, there are 4 formula units (*Z*) in a CuO unit cell and 8 in a Co_3O_4, which results the calculated density of CuO and Co_3O_4 are 6.30 and 6.02 grams/cm^3, respectively. The calculated average distance of Cu–O, Cu–Cu, Co–O and Co–Co are 1.97, 3.03, 1.93 and 3.11 Å, respectively. The fluctuated intensities in Fig. 1 could be influenced by the internal stress/strain change in the coating as indicated in our previous study [15]. The change of these mechanical properties is reaffirmed by the absence of metalic copper in the difractogram at annealing temperatures of 750 and 950 °C.

Basically, the detected oxides in XRD spectra practically arises from the calcination process toward the oxo bridge (M-O-M, with M=metal) formed from the sol-gel reaction hypothesized in the following schemes:

(i) Cu-O-Cu oxo bridge formation:

$$Cu(NO_3)_2.3H_2O + 2C_2H_5OH \xrightarrow{\textit{Alkoxide formation}} Cu(C_2H_5O)_2 + 3H_2O + 2HNO_3$$

$$Cu(OR)_2 + H_2O \xrightarrow{\textit{Hydrolysis}} OH\text{-}Cu\text{-}OR + ROH$$

$$OH\text{-}Cu\text{-}OR + OH\text{-}Cu\text{-}OR \xrightarrow{\textit{Condensation}} [OR\text{-}Cu\text{-}O\text{-}Cu\text{-}OR] + H_2O$$

$$OH\text{-}Cu\text{-}OR + OH\text{-}Cu\text{-}OR \xrightarrow{\textit{Condensation}} [OR\text{-}Cu\text{-}O\text{-}Cu\text{-}OH] + ROH$$

(ii) Co-O-Co oxo bridge formation:

$$Co(NO_3)_2.6H_2O + 2C_2H_5OH \xrightarrow{\textit{Alkoxide formation}} Co(C_2H_5O)_2 + 6H_2O + 2HNO_3$$

$$Co(OR)_2 + H_2O \xrightarrow{\textit{Hydrolysis}} OH\text{-}Co\text{-}OR + ROH$$

$$OH\text{-}Co\text{-}OR + OH\text{-}Co\text{-}OR \xrightarrow{\textit{Condensation}} [OR\text{-}Co\text{-}O\text{-}Co\text{-}OR] + H_2O$$

$$OH\text{-}Co\text{-}OR + OH\text{-}Co\text{-}OR \xrightarrow{\textit{Condensation}} [OR\text{-}Co\text{-}O\text{-}Co\text{-}OH] + ROH$$

(iii) Co-O-Cu oxo complex bridge formation:

$$OH\text{-}Cu\text{-}OR + OH\text{-}Co\text{-}OR \xrightarrow{\textit{Condensation}} [OR\text{-}Cu\text{-}O\text{-}Co\text{-}OR] + H_2O$$

$$OH\text{-}Cu\text{-}OR + OH\text{-}Co\text{-}OR \xrightarrow{\textit{Condensation}} [OH\text{-}Cu\text{-}O\text{-}Co\text{-}OR] + ROH$$

$$OH\text{-}Cu\text{-}OR + OH\text{-}Co\text{-}OR \xrightarrow{\textit{Condensation}} [OH\text{-}Cu\text{-}O\text{-}Co\text{-}OH] + ROR$$

where R = alkyl group (C_2H_5). The copper cobalt mixed oxides including spinels structure ($Cu_xCo_{3-x}O_4$) as directed in scheme (iii) do not appear in the XRD spectra. It may be due to the annealing temperature and the [Cu]/[Co] nitrate precursor ratio applied in this work

exceeded the critical conditions (350 ^{o}C; ratio of 0.5) [1, 16], resulting in separated copper and cobalt oxides which ultimately avoid or minimize the formation of spinel solid solution structure ($x \sim 0$).

3.2. Molecular dynamic (MD) simulation

The computer simulations can be used to understand the assemblies properties of molecules especially the microscopic interactions and structure [17]. There are two main classes of simulation techniques, namely Molecular Dynamics (MD) and Monte Carlo (MC) [18]. MD was developed to provide a thermodynamically accurate mesoscale model capable of elucidating non-equilibrium processes such as thermal shocks. The Planck constant is one of the most important factors in MD simulations [19, 20]. The Planck constant, *h*, is a physical constant that is the quantum of action, and can be generally expressed as $E = h\upsilon$, where E is energy and υ is the electromagnetic wave frequency. The other factor is volume, where Guggenheim [21] wrote the partition function, $\Delta(N, P, T)$, *as:*

$$\Delta(N, P, T) = \sum_{V} Q(N, V, T) e^{(-PV/k_B T)} \quad (1)$$

where k_B is Boltzmann constant, $Q(N, V, T)$ is the canonical ensemble partition function of a system composed of N particles held in a volume (V) and at a temperature (T), as well as external pressure (P) to which the system is exposed as the volume is permitted to change. The third factor is timing in which time-dependent statistical mechanic is vital to the MD simulation.

Based on these three parameters/factors, MD simulations were then executed to establish whether all these parameters are significant during the ionization process. The MD simulation and optimization results of CoOCo, CuOCu and CoOCu molecules are tabulated in Table 2, while the significance of the spots dispersion patterns during the ionization process are depicted in Fig. 3. Based on the ionization potential energies, the CoOCo seems to be the most stable structure, following by the CuOCu and the least stable is CoOCu. From these, it can be understood that the low probability presence of mixed cobalt copper oxide is due to the lowest ionization potential energy among the molecules.

3.3. Surface electronic structure

Fig.4 shows the XPS spectrum of Cu *2p* from copper oxide – cobalt oxide coating. The two main peaks of Cu $2p_{3/2}$ and Cu $2p_{1/2}$ are found without any satellites. The separation between the Cu $2p_{1/2}$ and Cu $2p_{3/2}$ peaks are around 20.0 eV which corresponds to the energy

difference between their each spin–orbit contribution. The absence of the satellites indicates that the electronic structure is dominated by low oxidation states of copper such as Cu(0) or Cu (I) [22].

The decoupling of Cu $2p_{3/2}$ peak gives two curve-fitting components as depicted in Fig. 5. The curve-fitting peak from binding energy of around 933.0 eV (62.7%) is from a tetrahedral Cu(I), while the octahedral Cu(II) is also present at the curve-fitting binding energy of around 933.6 eV as minor component (37.3%), with the ratio of Cu(II) to Cu(I) is 0.6. These observations reaffirm the cause of the absence of satellites in the Cu *2p* spectra as indicated. The type of sol precursor used in the solution preparation seems to influence the electronic structures of formed coating. In our previous work, copper acetate precursor was used and the satellites were formed [15], while it is no satellite detected in this report, even though they were relatively similar in the synthesis route.

The peak from octahedral Cu(I), as a counterpart of the tetrahedral, is not detected here. In the two or more system components, this may indicate that there is no strong interaction between the copper oxidation states with the oxidation states from other metal such as from cobalt [23]. It is expected that the copper oxides and cobalt oxides tend to separate to form their own metal oxides.

The profile of the Co *2p* spectra of copper oxide – cobalt oxide coating is shown in Fig. 6. The two main peaks of Co $2p_{3/2}$ and Co $2p_{1/2}$ and the weak satellites at high energy side of these main peaks are found. The weak satellites could indicate the presence of Co(II) ions as a minor component. Even though the existence of both Co(II) and Co(III) ions is confirmed by the asymmetry form of the Co $2p_{1/2}$ peak, the relatively weak Co $2p_{1/2}$ peak could indicate the presence of mixed Co(II,III) or Co_3O_4 bonding states. The decoupling of Co $2p_{3/2}$ peak would reaffirm these.

The decoupling of Co $2p_{3/2}$ peak provides four curve-fitting components as seen in Fig. 7. It is well accepted that the curve-fitting peak from binding energy of around 778.9 eV (37.9%) is from the octahedral Co(III), while the dominant curve-fitting peak from binding energy (BE) of around 781.1 eV (47.9%) is from the tetrahedral Co(II). These confirm the presence of Co_3O_4[1] with the Co(III) to Co(II) ratio of ~0.8. The minor curve-fitting peaks at BE of

around 783.9 eV (5.9%) and BE of around 787.0 eV (8.3%) are from Co(II) characteristic satellites.

Based on the Cu 2*p* and Co 2*p* spectra analyses, since the Co(III)/Co(II) ratio is less than unity and the species Cu(II) is the minor component, then there is low driving force for Cu(II) ions enter and partially replace the Co(II) sites in the Co_3O_4 structure to form the spinel (mixture) structure, eventhough they both have high similarity in diameter ($D_{Cu(II)}$ = 73 pm; $D_{Co(II)}$ = 74.5 pm) [1]. This is the cause of minimum formation (or possibly no-existing) of mixture oxides.

Fig. 8 shows the O *1s* XPS spectra of copper oxide – cobalt oxide film coating synthesized at 550 ^{o}C and its decoupling. The O *1s* spectra exhibit peak at BE of 530.4 eV with a big shoulder at BE peak around of 532.4 eV. This shoulder is capable of shifting the O *1s* peak from a normal position in the copper-cobalt system (BE around of 529.5 eV) [15, 23, 24] to 530.4 eV. This may be due to the different source of copper and cobalt sol precursors used. The decoupling of the O 1s photoelectron spectrum gives three curve-fitting components. The curve-fitting peak at BE of 530.2 eV (26.5%) attributes to the lattice O^{2-} (Cu–O, Co–O), the peak at BE of 531.4 (56.8%) may be treated as the surface oxygen from a wide variation of species such as adsorbed oxygen O^{-} and/or OH-like species, as hydroxyl, and carbonate groups, while the curve-fitting peak at BE around of 533.1 eV (16.75%) could be assigned as subsurface O^{-} species. Therefore, the big shoulder at the high energy side of O *1s* peak is due to the high percentage of the combination of surface and sub-surface oxygen.

Based on the elucidation of Cu *2p*, Co *2p* and the O *1s* XPS spectra, it can be generalized that the coating surface is dominated by Cu_2O, CuO, Co_2O_3 and CoO with minimum indication of mixed copper-cobalt spinel oxides formation. These compositions are quite different from the bulk/overall composition probed using XRD as seen in previous section. This is because the atmosphere significantly influences the surface electronic structure formation during the annealing process [23]. It is also significantly influenced by the sol precursors used as proven in our previous work with copper acetate and cobalt chloride precursors [15, 23, 24]

Fig. 9 shows the surface morphology of the coating probed using FESEM and AFM. FESEM result reveals that the surface is porous composed of interlinked nanoparticles (~10 to ~40 nm) which are partially agglomerated (Fig. 9a). AFM as contour identification (Fig. 9b) has

high consistency with the FESEM images which reveal a relief topographic with the presence of sharp small peaks and valleys. From the AFM image, the thickness of film coating per dip-drying cycle can be estimated using the peak-to-peak (Sy) parameter at around 40-50 nm [25]. The formation of homogeneous porosity of copper cobalt mixed oxide compound could be guided by the nitrogen adsorption – desorption mechanism (nitrogen from sol precursor or atmosphere) during the heating and calcination steps in the synthesis process [26].

3.5. Absorptance properties

The reflectance spectra of synthesized coatings with various dip-drying cycles are shown in Fig. 10. The absorptance value of each spectrum is determined using spectral distribution of terrestrial radiation at Air Mass (AM) 1.5 [27]. Aluminum substrates spectra, either before and after cleaning are also presented (Fig. 10a).

Low reflectance (< 20 %) in UV-Vis range and moderate reflectance (up to 70 %) in near infrared range (NIR) shown by the spectra (Fig. 10a-c). This indicates a solar selective absorber (SSA) curve profile are being approached. In Fig. 10a-c, there is a main trend: the thicker the film coatings (the more in the number of the dip-drying cycles) and the more concentrations of sol precursor, the higher the absorptance (α) values will be. This is in agreement with findings as reported by Bayon and co-researchers [9]. This indicates that the absorptance is directly influenced by the material properties and density. The highest absorptance (α = 91.93%) is achieved by the coating synthesized using [Cu]/[Co] ratio of 1 (0.25 M copper nitrate, 0.25 M cobalt nitrate) with 10 dip-drying deposition cycles. Nevertheless, the best absorptance is confined by a condition where the intersection point between the reflectance spectra and the cut-off line (at λ = 2.5μm) is at least above 50% of reflectance value leading to a minimum emittance condition [24]. Based on this, the best absorptance value is exhibited by the coating synthesized using [Cu]/[Co] ratio of 1 (0.1 M copper nitrate, 0.1 M cobalt nitrate) via 10 dip-drying cycles with the absorptance value of α = 88.7% (Fig. 10a). This result is very promising and exceeds the results achieved by sol-gel derived SSA coatings before the addition of an antireflection layer, namely α = 87% as reported by Bayon and co-researcher [9].

The wavy curves in the wavelength range of 0.6 - 1.7 μm which are consisted of the interference peak and the absorption edge [9] are the intrinsic characteristic of the coating due

to the interaction with certain light photon energy which depend on the coating thickness and the sol precursor concentration. The amplitude and the peak position of wavy curves tend to increase with the decrease of thickness of the coating (dip-drying cycle) and the decrease of sol precursor concentrations. Therefore, the presence of wavy curves is the direct function of the material density, thickness of coating as well as the reflectance properties of underlying substrate.

Low reflectance (or high absorption) in UV-Vis region could be due to the presence of numerous spin-allowed electron transitions (octahedral arrangements) between the partially filled *d*-orbitals in the coating material [23, 28]. Since these spin-allowed electrons do not have much effect on the infrared light, they produce low/moderate NIR absorption by the coating material. Reflectivity of aluminium substrate also plays important role in high reflectance of solar radiation.

Another factor influencing the absorptance of SSA is the porosity of coating [29]. Fig. 11 shows the reflectance spectra of copper cobalt oxide coatings deposited on aluminum substrate via electrospinning method for 2, 8 and 15 hour. Electrospining system leads to the formation of a micro-fiber network that eventually produces pore/void-rich coating [30]. It can be seen that the absorptance values are much lower than those absorptance values of coatings deposited by dipping method. This indicates that the pore/void effects are not a significant factor in improving the absortpance properties of the copper cobalt coating.

4. Conclusions

The structural and absorptance properties of copper and cobalt oxides composite coatings on aluminum substrates via sol-gel method have been successfully characterized using X-ray diffraction (XRD), X-ray photoelectron spectroscopy (XPS), field emission scanning electron microscopy (FESEM), atomic force microscopy (AFM), and UV-Vis-NIR spectrophotometer. XRD analyses revealed that the CuO and the Co_3O_4 composites were formed after the annealing process with the average difference of the calculated lattice parameters compared to ICDDs is 1.17%. MD simulation based on the hypothesized sol-gel reaction revealed that there was low indication of formation of copper-cobalt mixed phase oxides. Surface electronic structure mainly consisted of the tetrahedral Cu(I), octahedral Cu(II), tetrahedral Co(II), octahedral Co(III) as well as surface, sub-surface and lattice

oxygen O^-. Their composition are relatively balance, and no or minimum indication of mixed copper-cobalt/ spinel oxides formation. FESEM and AFM surveys revealed that the coating had a porous surface that is composed of interlinked nanoparticles (~10 to ~40 nm) which were partially agglomerated with a relief topograpic. UV-Vis-NIR reflectance spectra revealed that the increase of the dip-drying cycles in the coating preparation (which increases the thickness of the film) improved the absorptance (α) value. The similar trend is also exhibited by the increase of sol precursor concentrations. The optimum absorptance (α = 88.7%) was achieved when the coating was synthesized using copper and cobaalt nitrate sol concentration of 0.1 M deposited on aluminum substrate *via* 10 dip-drying cycles.

Acknowledgments

We gratefully acknowledge Dikti for funding *via* Hibah Kerjasama Luar Negeri Dikti 2016.

References

[1] D. Li, X. Liu, Q. Zhang, Y. Wang, H. Wan, Cobalt and copper composite oxides as efficient catalysts for preferential oxidation of CO in H2-rich stream, Catalysis Letters, 127 (2009) 377-385.

[2] A.S. Zoolfakar, R.A. Rani, A.J. Morfa, A.P. O'Mullane, K. Kalantar-Zadeh, Nanostructured copper oxide semiconductors: a perspective on materials, synthesis methods and applications, Journal of Materials Chemistry C, 2 (2014) 5247-5270.

[3] M. Zhang, R. Li, X. Chang, C. Xue, X. Gou, Hybrid of porous cobalt oxide nanospheres and nitrogen-doped graphene for applications in lithium-ion batteries and oxygen reduction reaction, Journal of Power Sources, 290 (2015) 25-34.

[4] R. Madhu, V. Veeramani, S.-M. Chen, A. Manikandan, A.-Y. Lo, Y.-L. Chueh, Honeycomb-like porous carbon–cobalt oxide nanocomposite for high-performance enzymeless glucose sensor and supercapacitor applications, ACS Applied Materials & Interfaces, 7 (2015) 15812-15820.

[5] C. Yuan, H.B. Wu, Y. Xie, X.W.D. Lou, Mixed transition-metal oxides: design, synthesis, and energy-related applications, Angewandte Chemie International Edition, 53 (2014) 1488-1504.

[6] K. Zhou, R. Wang, B. Xu, Y. Li, Synthesis, characterization and catalytic properties of CuO nanocrystals with various shapes, Nanotechnology, 17 (2006) 3939.

[7] S. Sun, Z. Wen, J. Jin, Y. Cui, Y. Lu, Synthesis of ordered mesoporous CuCo2O4 with different textures as anode material for lithium ion battery, Microporous and Mesoporous Materials, 169 (2013) 242-247.

[8] A. Amri, Z.-T. Jiang, N. Wyatt, C.-Y. Yin, N. Mondinos, T. Pryor, M.M. Rahman, Optical properties and thermal durability of copper cobalt oxide thin film coatings with integrated silica antireflection layer, Ceramics International, 40 (2014) 16569-16575.

[9] R. Bayón, G. San Vicente, C. Maffiotte, Á. Morales, Preparation of selective absorbers based on CuMn spinels by dip-coating method, Renewable Energy, 33 (2008) 348-353.

[10] B. Delley, From molecules to solids with the DMol 3 approach, The Journal of chemical physics, 113 (2000) 7756-7764.

[11] J.P. Perdew, K. Burke, M. Ernzerhof, Generalized gradient approximation made simple, Physical Review Letters, 77 (1996) 3865.

[12] S. Grimme, Semiempirical GGA-type density functional constructed with a long-range dispersion correction, Journal of Computational Chemistry, 27 (2006) 1787-1799.

[13] C. Braga, K.P. Travis, A configurational temperature Nosé-Hoover thermostat, The Journal of chemical physics, 123 (2005) 134101.

[14] K.P. Travis, C. Braga, Configurational temperature and pressure molecular dynamics: review of current methodology and applications to the shear flow of a simple fluid, Molecular Physics, 104 (2006) 3735-3749.

[15] A. Amri, Z.-T. Jiang, X. Zhao, Z. Xie, C.-Y. Yin, N. Ali, N. Mondinos, M.M. Rahman, D. Habibi, Tailoring the physicochemical and mechanical properties of optical copper–cobalt oxide thin films through annealing treatment, Surface and Coatings Technology, 239 (2014) 212-221.

[16] A. La Rosa-Toro, R. Berenguer, C. Quijada, F. Montilla, E. Morallon, J.L. Vazquez, Preparation and Characterization of Copper-Doped Cobalt Oxide Electrodes, The Journal of Physical Chemistry B, 110 (2006) 24021-24029.

[17] O.G. Jepps, G. Ayton, D.J. Evans, Microscopic expressions for the thermodynamic temperature, Physical Review E, 62 (2000) 4757.

[18] H. Zhao, N. Aluru, Molecular dynamics simulation of bulk silicon under strain, Interact. Multi. Mech, 1 (2008) 303-315.

[19] M.J. Uline, D.S. Corti, Molecular Dynamics at Constant Pressure: Allowing the System to Control Volume Fluctuations via a “Shell” Particle, Entropy, 15 (2013) 3941-3969.

[20] H.H. Rugh, Dynamical approach to temperature, Physical Review Letters, 78 (1997) 772.

[21] E. Guggenheim, Grand Partition Functions and So-Called``Thermodynamic Probability", The Journal of chemical physics, 7 (1939) 103-107.

[22] N. Pauly, S. Tougaard, F. Yubero, Determination of the Cu 2p primary excitation spectra for Cu, Cu 2 O and CuO, Surface Science, 620 (2014) 17-22.

[23] A. Amri, Z.-T. Jiang, P.A. Bahri, C.-Y. Yin, X. Zhao, Z. Xie, X. Duan, H. Widjaja, M.M. Rahman, T. Pryor, Surface Electronic Structure and Mechanical Characteristics of Copper−Cobalt Oxide Thin Film Coatings: Soft X-ray Synchrotron Radiation Spectroscopic Analyses and Modeling, The Journal of Physical Chemistry C, 117 (2013) 16457−16467.

[24] A. Amri, X. Duan, C.-Y. Yin, Z.-T. Jiang, M.M. Rahman, T. Pryor, Solar absorptance of copper–cobalt oxide thin film coatings with nano-size, grain-like morphology: Optimization and synchrotron radiation XPS studies, Applied Surface Science, 275 (2013) 127-135.

[25] A. Amri, Z.-T. Jiang, T. Pryor, C.-Y. Yin, Z. Xie, N. Mondinos, Optical and mechanical characterization of novel cobalt-based metal oxide thin films synthesized using sol–gel dip-coating method, Surface and Coatings Technology, 207 (2012) 367-374.

[26] S. Li, H. Wang, W. Li, X. Wu, W. Tang, Y. Chen, Effect of Cu substitution on promoted benzene oxidation over porous CuCo-based catalysts derived from layered double hydroxide with resistance of water vapor, Applied Catalysis B: Environmental, 166 (2015) 260-269.

[27] J.A. Duffie, W.A. Beckman, Solar Engineering of Thermal Processes, third ed., John Wiley & Sons Inc., New Jersey, 2006.

[28] N. Raman, S. Ravichandran, C. Thangaraja, Copper (II), cobalt (II), nickel (II) and zinc (II) complexes of Schiff base derived from benzil-2, 4-dinitrophenylhydrazone with aniline, Journal of Chemical Sciences, 116 (2004) 215-219.

[29] E. Ienei, L. Isac, C. Cazan, A. Duta, Characterization of $Al/Al_2O_3/NiO_x$ solar absorber obtained by spray pyrolysis, Solid State Sciences, 12 (2010) 1894-1897.

[30] I.S. Chronakis, Novel nanocomposites and nanoceramics based on polymer nanofibers using electrospinning process—a review, Journal of Materials Processing Technology, 167 (2005) 283-293.

Figures:

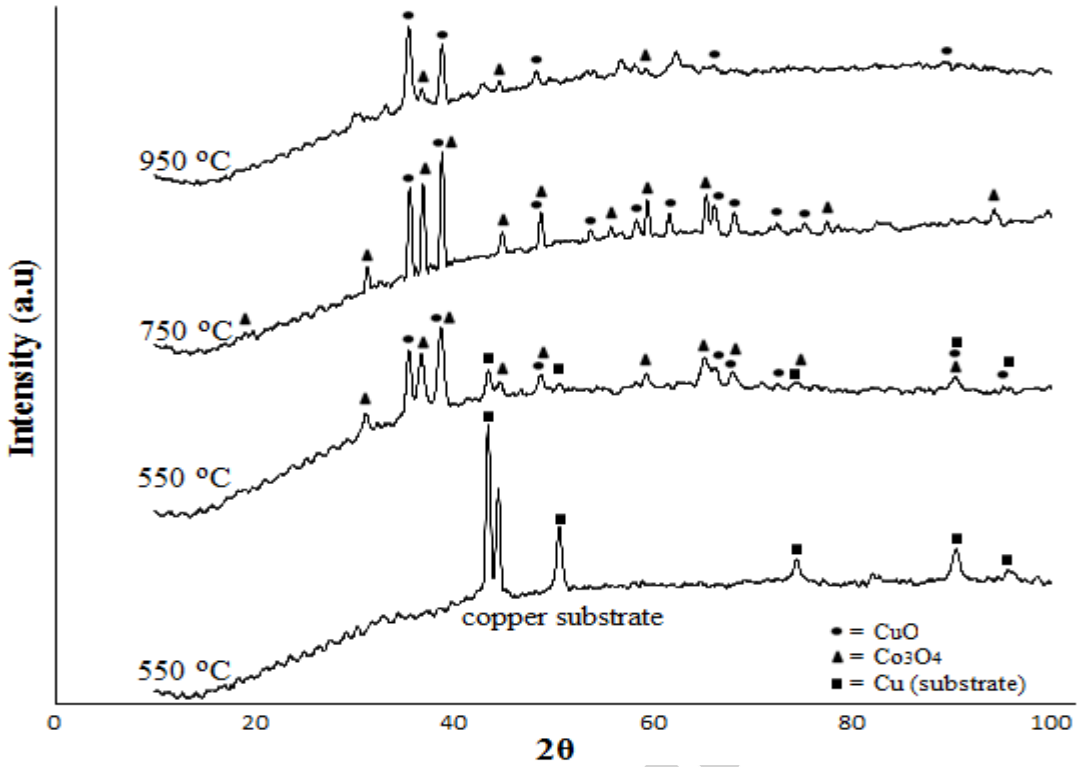

Fig. 1. XRD pattern of copper oxide – cobalt oxide coatings on copper substrate synthesized using nitrate based sol precursors on copper substrate at different annealing temperatures.

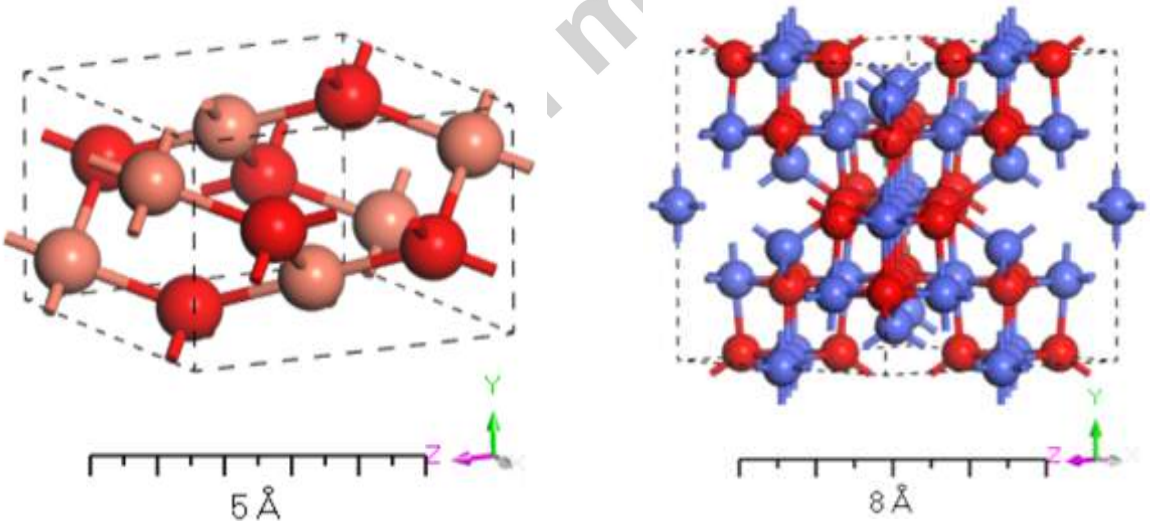

CuO Co_3O_4

Fig. 2. The coexist crystal structures. Brown, red and blue are Cu, O and Co atoms, respectively

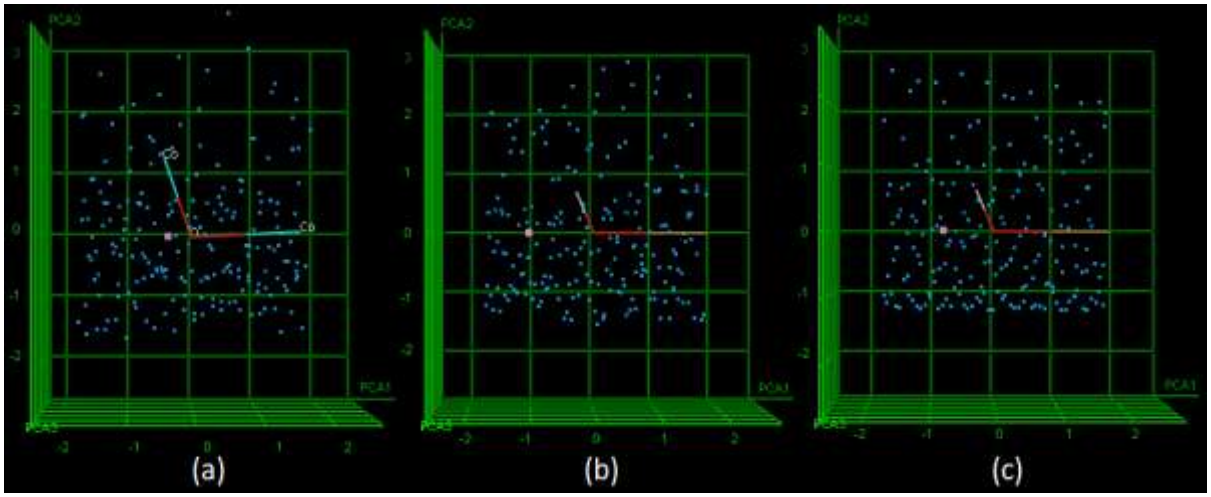

Fig. 3. The ionization process of: (a). CoOCo, (b). CuOCu, (c). CoOCu

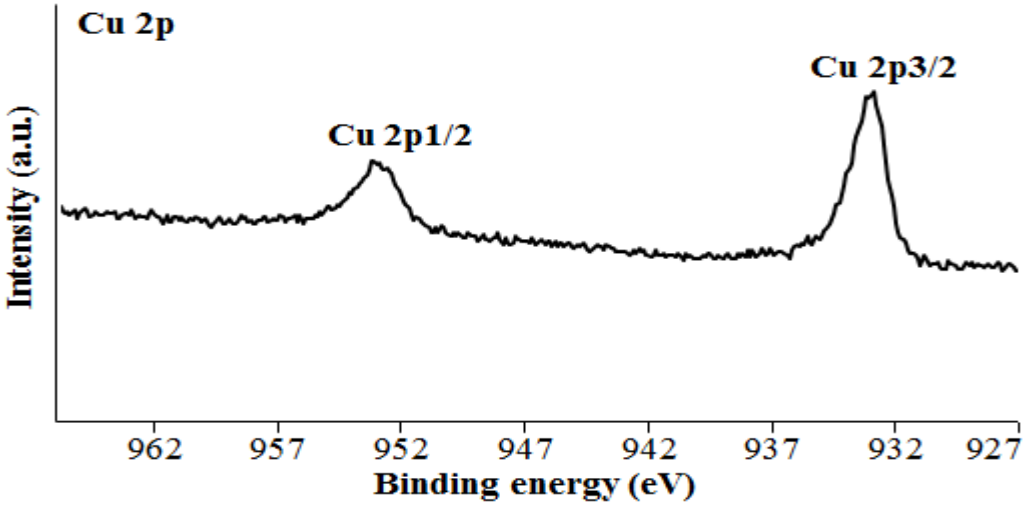

Fig. 4. High resolution Cu *2p* XPS spectrum from of copper oxide – cobalt oxide film coating annealed at 550 ^{o}C.

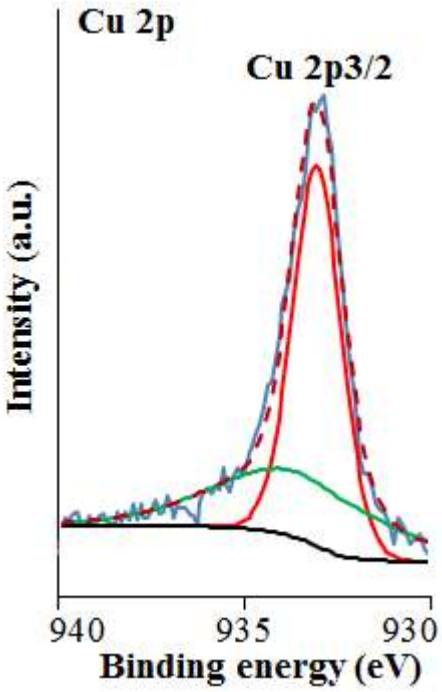

Fig. 5. Decoupling of Cu $2p_{3/2}$ peaks from copper – cobalt oxide film coating annealled at 550 ^{o}C.

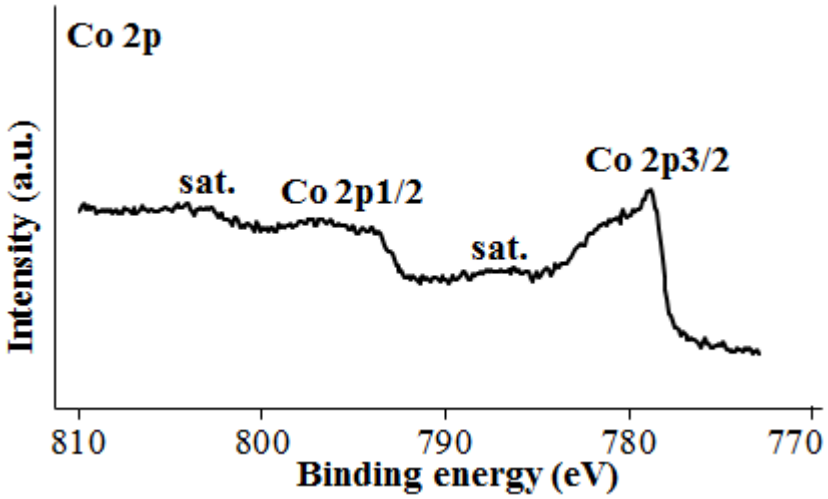

Fig. 6. Co *2p* XPS spectrum of copper oxide – cobalt oxide film coating synthesized at annealing temperature of 550 ^{o}C.

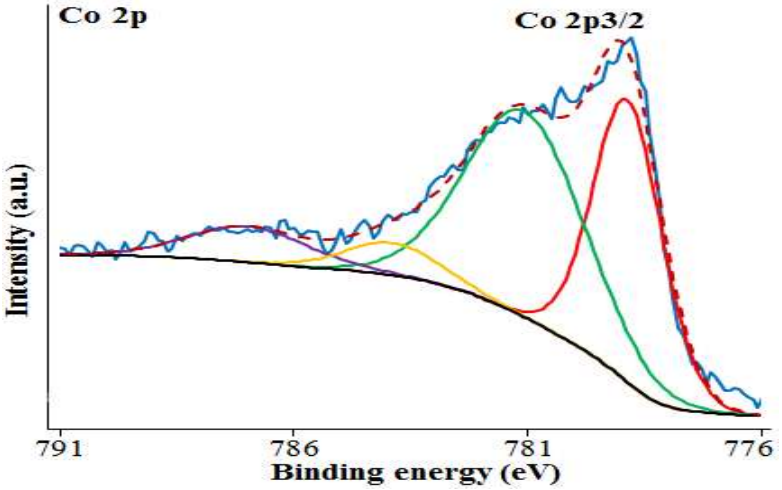

Fig. 7. Decoupling of Co $2p_{3/2}$ peaks of copper – cobalt oxide film coating synthesized at annealling temperture of 550 ^{o}C.

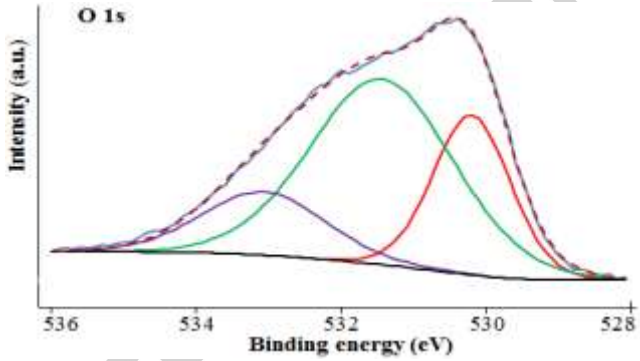

Fig. 8. The 0 1s XPS spectra of coating annealed 550 ^{o}C and its curve-fitting.

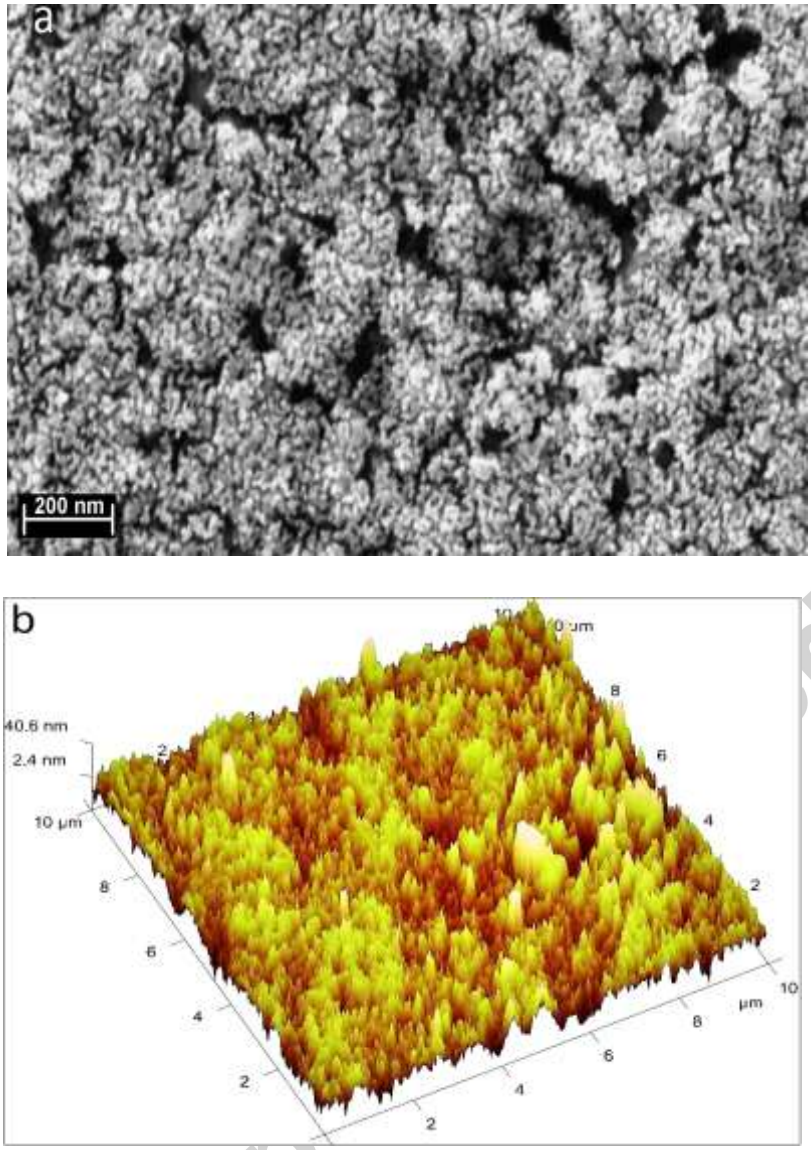

Fig. 9. Surface morphology of coating synthesized at annealing temperatures of 550 ^{o}C investigated *via* (a) FESEM, and (b) AFM.

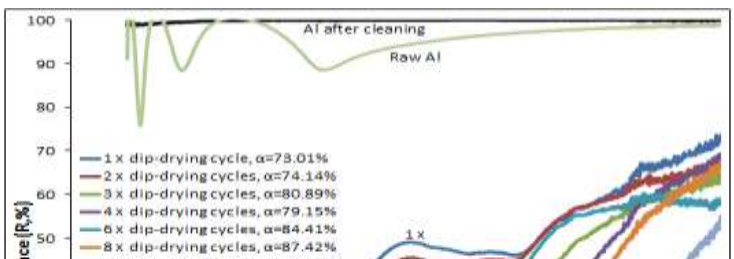

Fig. 10. Reflectance spectra of copper cobalt oxide thin film coatings on aluminium substrates synthesized using copper to cobalt mol ratio 1:1 at concentrations of: a) 0.1M, b) 0.25M, c) 0.4M with corresponding solar absorptance (α) values.

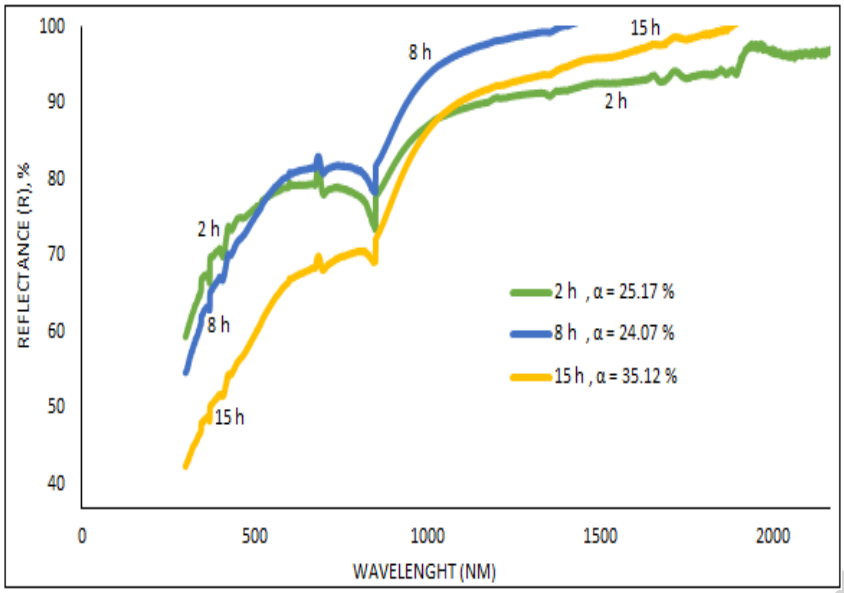

Fig. 11. Reflectance spectra of copper cobalt oxide coatings deposited on aluminum substrate *via* electrospinning method for 2, 8 and 15 hour.

Tables:

Table 1. The coexist crystal structures.

	Space group	Calculated lattice parameters (*a*, *b*, *c*, *β*)	Calculated atoms site (fractional coordinate)	ICDD	Lattice parameters in ICDD (*a*, *b*, *c*, *β*)
CuO	C2/c (15)	4.67 Å, 3.55 Å, 5.15 Å, 100.03°	Cu: 0.25, 0.25, 0.00 O: 0.00, 0.42, 0.25	00-045-0937	4.6853 Å, 3.4257 Å, 5.1303 Å, 99.5490°
Co_3O_4	Fd-3m (227)	8.10 Å	Co: 0.13, 0.13, 0.13 Co: 0.50, 0.50, 0.50 O: 0.26, 0.26, 0.26	01-080-1533	8.0968 Å

Table 2. The optimized parameters from MD simulation.

Molecules	Factors/Parameters			
	Time (s)	Temperature (K)	Pressure (Bar)	Ionization Potential (eV)
CoOCo	1500	69.602	183998	0.93
CuOCu	3000	64.436	230450	0.76
CoOCu	15000	53.175	94496	0.39